themselves to be susceptible to these thermally induced phase transformations.[29]

Conclusions

A combination of materials characterization techniques can be successfully used to develop the relationship between stacking patterns of these disklike molecules and their optical and electronic properties. The theory for exciton formation in condensed phase chromophores (smaller molecules than the phthalocyanines) has been extensively developed.[23,24] Splitting of the normally degenerate excited-state energies occurs when a dimer structure is achieved for the planar aromatic centers in close proximity, which eventually leads to a "band structure" in extended aggregates. It is clear that for cofacially, collinearly aligned aromatic centers (just the dimeric unit) that the parallel transition dipoles in the excited state result in preferential population of the higher energy excited state (blue shifting of the absorbance spectrum). This is indeed seen for certain solution aggregates of metal-Pc's and for synthesized cofacial (O-Si-O)-Pc dimers and trimers.[23,26] This same relationship may be operative in the cofacially aligned GaPc-Cl and VOPc aggregates. In-line transition dipoles of simple chromophore aggregates lead to preferential population of the lower energy in the excited state (red shifting of the absorbance spectrum, as for J aggregates of certain cyanine dyes[24]). Last, transition dipoles aligned obliquely with respect to each other can lead to population of both upper and lower excited-state manifolds which leads to simple splitting of the absorbance band.[24] While the picture for the cofacially stacked linear Pc aggregates is reasonably clear (blue-shifted and broadened spectra result), it is still not clear whether the red shifting and broadening seen for the platelet-phase VOPc and GaPc-Cl systems is due to an already characterized transition dipole model.

It is surprising to see that Ag^0 nuclei decoration of the block/prismatic phase of GaPc-Cl at 640-nm irradiation does not result in observable decoration of the platelet form—even though appreciable spectral overlap is likely and energy transfer is certainly favored. Irradiation at 800 nm is apparently capable of decorating both crystal types, which is consistent with the notion that the absorbance spectrum of the block/prismatic phase of GaPc-Cl extends well into this wavelength region (Figure 5a). The Ag^0 nuclei decoration experiments and our recent microcircuit photoconductivity measurements[29] indicate a higher degree of photoactivity for the platelet (slipped-stack) phase of both the tetravalent and trivalent metal Pc's. If we assume that their surface electrochemistries are comparable for Ag^0 deposition, we conclude that exciton transport and/or charge generation and transport in this slipped-stack configuration of the cofacial Pc's is more efficient than for the linear, cofacially aligned Pc's. Since the photoconductive process is extremely sensitive to the presence of trace dopants in the aggregated Pc's, it is difficult at present to distinguish which mode is more important. Studies are under way to develop more ordered layers of these Pc's, with which these questions can be more fully answered.

Acknowledgment. This research was supported by grants from the National Science Foundation, CHE86-18181 and CHE86-14955, and by the Materials Characterization Program—State of Arizona. The technical support of Patrick Epperson and Wayne Punjak is also gratefully acknowledged.

---

(29) Lee, P.; Armstrong, N. R., unpublished results.

In Situ Pore Structure Studies of Xerogel Drying

Christopher L. Glaves,[†] C. Jeffrey Brinker,[‡] Douglas M. Smith,[*,†] and
Pamela J. Davis[†]

UNM Center for Micro-Engineered Ceramics, The University of New Mexico, Albuquerque,
New Mexico 87131, and Division 1846, Sandia National Laboratories, Albuquerque,
New Mexico 87185

Received May 20, 1988

Low-field spin-lattice relaxation (20 MHz proton NMR) measurements of ethanol contained in two base-catalyzed silica xerogels aged under different conditions have been applied as an in situ probe of pore structure development during xerogel drying. Two base-catalyzed silica gels were prepared and aged under different conditions. One sample (designated E) was aged in pure ethanol for 1 week and the second (designated B) in an ethanol-KOH mixture for the same time period prior to drying. 180°-τ-90° relaxation experiments were performed at 20 MHz and 303 K as each gel dried. In addition, gel shrinkage and weight loss were monitored. After complete drying, the surface area and pore size distribution of each sample were obtained from nitrogen adsorption/condensation. During drying, a gradual pore shrinkage for both samples was observed until the structures stiffened, causing the fluid meniscus to penetrate the pores. For sample E, this caused the surface area to decrease from $\approx$1000 to 600 m^2/g and microporosity development in the pore size distribution. For sample B, the surface area decreased from $\approx$1500 to 200 m^2/g and microporosity disappeared. The final NMR-derived pore size distributions were in good agreement with that obtained from nitrogen condensation.

Introduction

During xerogel synthesis, aging and drying are crucial steps in the development of the final physical structure. Depending upon the aging conditions (i.e., temperature, pH, time, solvent) and the drying conditions (i.e., time-temperature), the structure of the product xerogel and, hence, its properties may be significantly altered.[1] In general, the effect of changing a processing condition has

---

[*] Author to whom correspondence should be addressed.

[†] The University of New Mexico.

[‡] Sandia National Laboratories.

(1) Scherer, G. W. *J. Non-Cryst. Solids* **1988**, *100*, 77.

0897-4756/89/2801-0034$01.50/0 © 1989 American Chemical Society

been assessed by examining the structure of the final xerogel and inferring the mechanisms that have caused the changes. Since xerogels are the subject of increased interest as a result in their role in sol–gel processing of ceramics, a better understanding of physical structure changes *during drying* is desirable.

Aging of gels normally refers to the temporal changes that take place after the gel point but prior to drying. According to a recent review by Scherer[1] these chemical and structural changes may be categorized as (1) hydrolysis (replacement of alkoxide groups with hydroxyl groups plus alcohol formation) or the reverse reaction reesterifications, (2) polymerization (condensation reactions involving the hydroxyl groups to produce M–O–M bonds plus water or alcohol) or the reverse reactions, depolymerization, (3) syneresis (spontaneous gel shrinkage that occurs by expulsion of solvent), and (4) coarsening (dissolution and reprecipitation that results in a reduction of solid–liquid interfacial area).

Drying occurs by solvent evaporation in two stages. Initially the gel is able to shrink to remain filled with solvent (thus avoiding high-energy solid–vapor interfaces in the gel). The shrinking gel becomes increasingly stiffer, so that at some point it can no longer shrink to accommodate the leaving solvent. In the second stage, liquid–vapor menisci develop and penetrate the gel. The gel stops shrinkage at the point where the menisci develop their maximum curvature, causing the capillary pressure, which exerts a compressive stress on the gel, to be maximized.

The phenomena that we ascribe to aging (for example, polymerization) may continue to occur during drying. These aging effects, whether they occur before or during drying, influence the dried gel (xerogel) pore structure. If aging results in greater polymerization, the gel network will be stiffer, causing it to stop shrinking at an earlier stage of drying. This results in a more porous xerogel. Conversely if aging causes reesterification of the hydroxyl groups, subsequent polymerization is precluded. The gel then is able to shrink much more before it is stiff enough to withstand the capillary pressure (which is now enormous due to the smaller menisci). The resulting xerogel is quite dense and contains very tiny pores.

Coarsening is the accepted method of stiffening a gel structure. The gel is aged under conditions where the depolymerization rate is appreciable. Convex surfaces are more soluble (undergo depolymerization more rapidly) than concave surfaces. Therefore material is removed from convex surfaces and reprecipitated at concave surfaces. It is thought that this coarsening process grows necks between touching particles or clusters, increasing stiffness, decreasing surface area, and reducing drying shrinkage. Coarsening or "Ostwald ripening" is discussed at length by Iler.[2]

Most pore structure analysis techniques (i.e., adsorption/condensation, mercury porosimetry, transmission electron microscopy) are not appropriate for the study of structural changes during drying since they require the removal of pore fluid before analysis. Since structural changes during drying are the object of study, a nonintrusive technique that probes pore structure of "wet" materials is required. Thermoporometry is applied to pore structure analysis for wet materials.[3] This method has been applied to gel characterization,[4] but it is not nonintrusive in the sense that the sample temperature must be changed during the analysis and phase changes occur in the sample (the basis of the method) that can cause structural change in the gel. Of particular utility for this study is the use of low-field NMR spin–lattice relaxation measurements of pore fluid. The basic principle is that fluid in the close proximity of a surface undergoes spin–lattice relaxation at a faster rate than the corresponding bulk fluid.[5,6] Recently, NMR pore structure analysis has been applied to a range of porous solids.[7-12] The technique's popularity arises from the ability to study wet solids, lack of pore network/percolation effects (which limit mercury porosimetry, N_2 condensation, thermoporometry), no pore shape assumption, rapid analysis, wide pore size range, and the potential for nonintrusive in situ analysis.

For a porous solid with a distribution of pore sizes (which each have a characteristic T_1), the observed magnetization will depend on the distribution of pore volume with T_1, $f(T_1)$:

$$\mathbf{M}(\tau) = \mathbf{M}_0 \int_{T_{1_{\min}}}^{T_{1_{\max}}} [1 - 2\exp(-\tau/T_1)] f(T_1)\, \mathrm{d}T_1 \qquad (1)$$

The distribution of pore volume with respect to T_1 is related to the desired pore size distribution (PSD). Equation 1 must be deconvoluted to extract $f(T_1)$ from the $\mathbf{M}(\tau)$ measurements. Munn and Smith[13] have used the nonnegative least-squares (NNLS) method of Lawson and Hanson[14] to obtain discrete T_1 distributions, and several investigators[11,12] have used the method of regularization to extract continuous distributions.

For the pore fluid conditions in gel drying, diffusion between the surface and bulk phases is fast as compared to relaxation. Therefore, the observed relaxation time, T_1, is related to the T_1's of the surface and bulk phases and the respective volume of fluid in each phase by the "two-fraction, fast-exchange" model:[15]

$$1/T_1 = f_b/T_{1_b} + f_s/T_{1_{\mathrm{surface}}} \qquad (2)$$

Defining the pore size as the pore hydraulic radius ($r_p = 2V_p/A_s$), eq 2 may be rewritten for saturated pores greater than ≈5 nm:[7]

$$1/T_1 = 1/T_{1b} + 2/(T_{1_s} r_p) \qquad (3)$$

T_{1_b}, the relaxation time of the bulk fluid, depends on the fluid and temperature. T_{1_s}, the ratio of surface relaxation time and thickness of the surface-affected phase (1–2 monolayers[16,17]), is a function of temperature, fluid, proton frequency, and surface chemistry. Equation 3 is often given[7,12] as

$$1/T_1 = \alpha + \beta/r_p \qquad (4)$$

---

(2) Iler, R. K. *The Chemistry of Silica*; John Wiley and Sons: New York, 1979.

(3) Brun, M.; Lallemand, A.; Quinson, J. F.; Eyraud, C. *Thermochim. Acta* **1977**, *21*, 59.

(4) Quinson, J. F.; Dumas, J.; Serughetti, J. *J. Non-Cryst. Solids* **1986**, *79*, 379.

(5) Brown, R. J. S. *Bul. Am. Phys. Soc., Ser II* **1956**, *1*, 216.

(6) Senturia, S. D.; Robinson, J. D. *Soc. Pet. Eng. J.* **1970**, *10*, 268.

(7) Gallegos, D. P.; Munn, K.; Smith, D. M.; Stermer, D. L. *J. Colloid Interface Sci.* **1987**, *119*, 127.

(8) Schmidt, E. J.; Velasco, K. K.; Nur, A. M. *J. Appl. Phys.* **1986**, *59*, 2788.

(9) Glaves, C. L.; Davis, P. J.; Gallegos, D. P.; Smith, D. M. *Energy Fuels*, **1988**, *2*, 662.

(10) Gallegos, D. P.; Smith, D. M.; Brinker, C. J. *J. Colloid Interface Sci.* **1988**, *124*, 186.

(11) Gallegos, D. P.; Smith, D. M. *J. Colloid Interface Sci.* **1988**, *122*, 143.

(12) Brown, J. A.; Jackson, J. A.; Brown, L. F.; Milewski, J. V.; Travis, B. J. *Proc. SPE/DOE Unconventional Gas Recovery Symp.* **1982**, 203.

(13) Munn, K.; Smith, D. M. *J. Colloid Interface Sci.* **1987**, *119*, 117.

(14) Lawson, C. L.; Hanson, R. J. *Solving Least Squares Problems*; Prentice-Hall: Englewood Cliffs, NJ, 1982.

(15) Brownstein, K. R.; Tarr, C. E. *J. Magn. Reson.* **1977**, *26*, 17.

(16) Woessner, D. E. *J. Magn. Reson.* **1980**, *39*, 297.

(17) Almagor, E.; Belfort, G. *J. Colloid Interface Sci.* **1978**, *66*, 146.

where α is $1/T_{1_b}$ and β is $2/T_{1_s}$. For pores less than 5 nm in radius, a pore geometry assumption is necessary. Expressions have been reported for flat plate, cylindrical, and spherical cavity pores and the void space in a packing of solid spheres.[10] For pores less than $\approx$0.5 nm, the two-fraction, fast-exchange model has no physical significance, and this represents the lower size limit for which a distribution of pore sizes may be determined. However, the fraction of the total pore volume with size less than 0.5 nm may still be obtained.

For pore size analysis, the problem of obtaining values for α and β remains. Glaves and co-workers[18] have shown that by using the same sample with different amounts of fluid, T_{1_b} and T_{1_s} (or α and β) may be directly determined if A_s is known from another method (usually from adsorption). For low fluid content, single-exponential magnetization is usually observed and T_1 is given by[19]

$$1/T_1 = \alpha + \beta A_s M_v/2 \qquad (5)$$

where M_v is the solid mass per volume of fluid adsorbed (for saturated pores, M_v equals $1/V_p$). By varying the adsorbate loading and measuring T_1, a plot of $1/T_1$ versus $A_s M_v$ will be linear with a slope of $\beta/2$ and intercept of α. If the sample has a wide pore size distribution and a range of small pores are saturated, single-exponential decay may not be observed, and β is determined by[19]

$$\beta = (2/[A_s M_v])\sum_{j=1}^{n} f(T_{1_j})[1/T_{1_j} - \alpha]\Delta T_{1_j} \qquad (6)$$

Experimental Section

Silica sol–gel samples were prepared via a two-step base-catalyzed process using tetraethyl orthosilicate (TEOS) designated as B2.[20] Gels were cast in NMR tubes as right cylinders. After gelation, one sample was aged for 7 days in an excess of 0.05 M solution of dry KOH in absolute ethanol, while the other sample was aged for the same period in an excess of absolute ethanol alone. The purpose of the investigation was to understand the effects of coarsening or reesterification during aging on the subsequent drying step. The KOH strength used for the base-aged gel was chosen according to a series of screening experiments designed to find a condition that changed the relaxation behavior of the gel while still leaving it structurally intact. A 0.05 M solution of KOH in EtOH met this criterion. After aging, both samples were removed from the solution, weighed, and sealed in 5-mm NMR tubes. The samples were then slowly dried at 303 K over a period of about 2 weeks via small holes in the NMR tube caps. Upon drying, the samples did not remain attached to the tube walls and appeared to shrink unhindered by interactions with the tube. The sample length was measured optically in the NMR tube after each NMR experiment.

NMR spin-lattice relaxation inversion recovery (180°–τ–90°) experiments were performed on the fluid-containing samples periodically during the drying process. NMR measurements were performed at a proton frequency of 20 MHz on a spin-lock CPS-2 pulse NMR equipped with a 4.7-kG magnet. The magnet and sample space were held at a temperature of 303 K in an insulated air space surrounded by a constant-temperature water bath. Magnetization relaxation curves were obtained by measuring the height of the free induction decay curve (FID) at approximately 30–50 different τ values between 10 μs and 9 s. Averaging was used to obtain the FID at each τ, with two pulse sequence FIDs averaged per τ for most samples and four or eight averaged for samples with poor signal-to-noise ratios. Data collection was facilitated by the use of a Hitachi VC-6041 digital storage oscilloscope interfaced with an IBM CS 9000 microcomputer.

Before each relaxation experiment, sample weight and length were recorded. At approximately 99% solvent loss, KOH-aged and EtOH-aged samples were dried completely in an oven at 323 K. Nitrogen adsorption/condensation measurements were performed on the dry samples using an Autosorb-1 adsorption analyzer to calculate dry sample surface areas and pore size distributions. Samples were outgassed under vacuum at 323 K for approximately 1 h prior to measurement, and five adsorption points in the relative pressure range of 0.05–0.31 were used for BET surface area analysis. The nitrogen cross-sectional area was taken as 0.162 nm^2. Pore radius distributions for pore radii greater than 1 nm were calculated from the desorption branch of the nitrogen isotherms.

Following nitrogen adsorption/condensation analysis, the dried samples were resaturated with absolute ethanol in an atmospheric desiccator. Ethanol uptake (determined gravimetrically) coincided with the total pore volume from nitrogen condensation, indicating that the sample was completely saturated and that, as expected, the samples did not swell upon reintroduction of the ethanol. NMR inversion recovery experiments were again performed to obtain sample pore size distributions for comparison with the nitrogen adsorption/condensation analysis. α and β determination was made by performing subsequent NMR inversion recovery experiments on the samples at several different levels of ethanol saturation (the surface area method). Different saturation levels were attained by allowing the ethanol-resaturated samples to dry to a weight corresponding to the desired saturation. This was followed by a period of equilibration at experimental temperature (303 K) before performing the NMR measurements. In addition to relaxation experiments on pore fluids, separate T_1 measurements were conducted on bulk ethanol and ethanol/KOH as well as gels before and after the gel point. These results reaffirmed that changes in T_1 in the gels were the result of pore structure only.

Data from the NMR experiments were deconvoluted into T_1 distributions by using the nonnegative least-squares routine[13] for discrete distributions and via regularization[11] for continuous distributions. An optimum smoothing parameter, δ, was found for most distributions deconvoluted from the magnetization data via regularization. For calculation of pore size distributions, a cylindrical pore shape assumption was used. The effect of this assumption is a strong function of the pore size as discussed by Gallegos and co-workers.[10]

Results and Discussion

The samples were placed in NMR tubes and allowed to attain thermal equilibrium at the experiment temperature (303 K). Then, a relaxation experiment was performed. The T_1 distribution had a single maximum, and a volume-average relaxation time, $T_{1_{av}}$, was calculated from the NNLS-derived distribution by using eq 6. $T_{1_{av}}$ of $\sim$1.1 s for the KOH-aged sample and $\sim$1.5 s for the sample aged in EtOH were obtained. This compares with a T_1 for pure ethanol of $\sim$2.1 and $\sim$1.9 s for a mixture of 90% ethanol/10% water. As the samples dried, relaxation experiments were periodically performed. For solvent weight losses less than $\sim$65% of the total solvent content, single-exponential behavior was noted. For higher solvent losses, a second peak was observed with a T_1 on the order of 0.1 s. The variation of $T_{1_{av}}$ with solvent weight loss is presented in Figure 1. A continual decrease of $T_{1_{av}}$ with decreasing solvent content is noted for both samples, with the sample aged in KOH always having a lower $T_{1_{av}}$ for a given solvent content. This decrease in $T_{1_{av}}$ can be the result of higher surface area, lower pore volume, and/or decreasing saturation of the pores. However, from sample length and weight measurements, these different possible mechanisms may be identified.

The T_1 distribution resulting from each experiment can be translated into a sample pore size distribution (for fully saturated samples) and/or a sample surface area (for fully or partially saturated samples) once the α and β values are

---

[18] Glaves, C. L.; Davis, P. J.; Smith, D. M. *Powder Technol.* **1988**, *54*, 261.

[19] Davis, P. J.; Gallegos, D. P.; Smith, D. M. *Powder Technol.* **1987**, *53*, 39.

[20] Brinker, C. J.; Keefer, K. D.; Schaefer, D. W.; Ashley, C. S. *J. Non-Cryst. Solids* **1982**, *48*, 47.

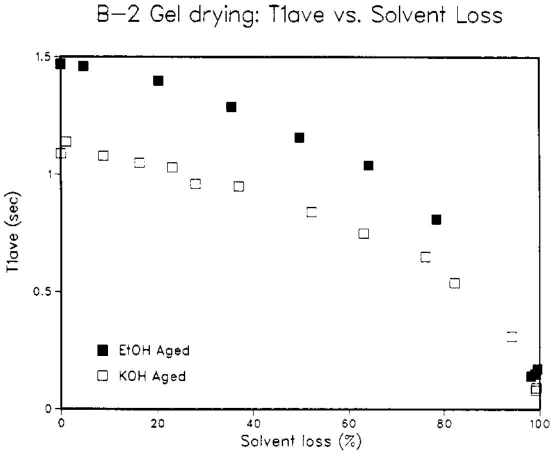

Figure 1. Variation of the average relaxation time as a function of solvent drying.

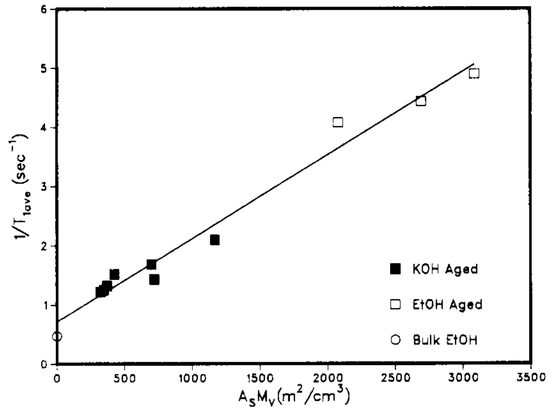

Figure 2. Surface area–concentration plot for the determination of α and β.

known for the experimental conditions. α and β were calculated from the experiments at different ethanol resaturation levels via the surface area method. Figure 2 is a plot of $1/T_{1_{av}}$ versus A_sM_v as measured in these experiments. The surface areas used to construct the A_sM_v plot, obtained via nitrogen adsorption on dry samples, were 230.4 m^2/g for the KOH-aged sample and 627.5 m^2/g for the EtOH-aged sample. However, we should note that based on the adsorption isotherms, both samples, and in particular the EtOH-aged sample, exhibited microporosity. The use of the BET equation for materials with microporosity can lead to increased uncertainty in the calculated surface area.[21] A least-squares fit of the data presented in Figure 2 in conjunction with eq 5 yields α equal to 0.684 s^{-1} and β equal to 2.83 nm/s. The fact that the data from both samples approximately fit the same line is an indication of similar surface chemistry for the two samples. The value of β is very close to that reported by Gallegos et al.[10] for water relaxation at 20 MHz and 303 K on similar silica xerogels. Glaves and co-workers[18] have shown that at low field strengths, ethanol and water have very similar surface-enhanced spin–lattice relaxation behavior. The presence of any water remaining in the ethanol pore fluid will have a minor effect on the observed T_1 because of this similarity. Although both the surface area and surface morphology of the samples are changing during the drying process, past experience using materials with a range of surface roughness and area[18,19] lead us to conclude that β should be fairly constant during drying. The value of α derived from the intercept in Figure 2 (i.e., the extrapolation of eq 5) is slightly larger than the inverse of bulk T_1 for pure ethanol. However, this is commonly observed[7,9] and is probably the result of the pore fluid not having the same exact composition as the bulk fluid.

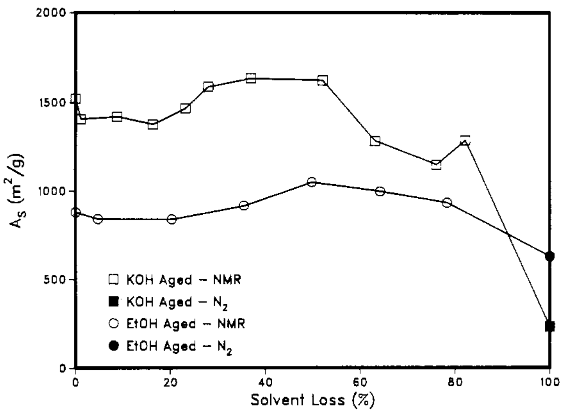

Figure 3. Variation of surface area as a function of drying.

The discrete T_1 distribution from NNLS were used in conjunction with α and β to calculate sample surface areas during the drying process.[19] The variation in surface area as a function of solvent loss is presented in Figure 3. We should note that this in situ surface area determination is not normally available by conventional techniques. To use adsorption techniques, one would have to completely remove the solvent *before* surface area analysis and thus (based on Figure 3) change the surface area. For thermoporometry, the pore fluid must be a single pure fluid, which requires repeated exchanging of pore fluid. This allows an in situ probe but can result in changes in pore structure during the fluid-exchange process and during the required temperature changes of the analysis.

Two findings in Figure 3 are surprising. The very large surface areas for both samples (800–1500 m^2/g) are indicative of very small features (and/or microporosity) that are not observed in the N_2 surface areas obtained on the dried samples. This finding is consistent with small-angle X-ray scattering results that indicate that B2 gels are mass fractals.[20] The uncertainty in surface area determination is on the order of 5% at low solvent loss and increases to $\approx$10% as the sample dries. The general trend of a slight increase in surface area with drying and a surface area maximum in the region of 40–50% solvent loss was consistently observed. The observation that the surface area for the KOH-aged sample was larger than that for the EtOH-aged sample for the first 80% of solvent loss was not anticipated. However, the higher surface area measured for the KOH-aged gel is corroborated by a small-angle X-ray scattering experiment performed by Schaefer and Brinker.[22] Before drying, the EtOH-aged sample exhibited a Porod slope of −1.81, indicative of a mass fractal object with fractal dimension $D = 1.81$. (The fractal dimension, D, relates the objects mass, M, to its radius, r, according to $M \propto r^D$, where in three dimensions, $D < 3$). This value is slightly lower than values reported elsewhere for gels made under similar conditions.[23] The KOH-aged sample exhibited a Porod slope of −3.01, indicative of a surface fractal object with surface fractal dimension $D_s = 2.91$. (The surface fractal dimension relates an objects surface area, S, to its radius according to $S \propto r^{D_s}$, where D_s varies from 2 for a minimal surface to

---

(21) Lowell, S.; Shields, J. *Powder Surface Area and Porosity*, 2nd ed.; Chapman and Hall: London, 1984.

(22) Schaefer, D. W., Brinker, C. J., manuscript in preparation.

(23) Brinker, C. J.; Scherer, G. W. *J. Non-Cryst. Solids* **1985**, *70*, 301.

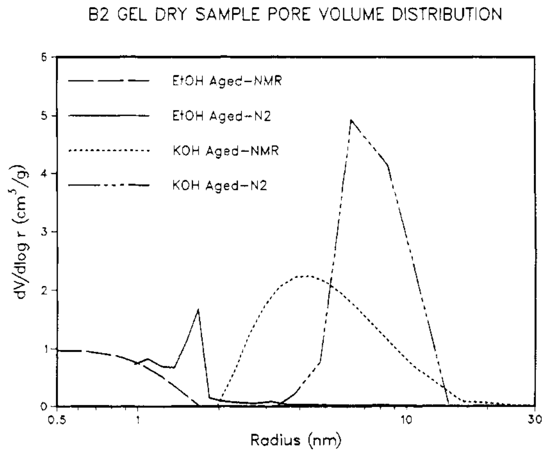

Figure 4. NMR and nitrogen condensation (desorption branch) derived pore size distributions on gel samples after drying.

3 for a surface so convoluted that it fills three-dimensional space). KOH aging apparently caused a restructuring of the mass fractal to create a surface fractal with an extremely rough surface. Because coarsening is thought to occur by a dissolution–reprecipitation process that results in a reduction in surface area, this opposite effect is quite surprising, especially when considering that the shrinkage was significantly reduced as generally expected for a coarsening process. The mechanistic details of this coarsening/roughening process are currently under investigation. It is also worthwhile to note that aging in a large excess volume of ethanol caused the EtOH-aged sample to shrink more during drying than the corresponding gel aged in its mother liquor (EtOH + H_2O). This suggests that EtOH aging causes some reesterification, which (as discussed in the Introduction) promotes shrinkage during drying. Direct evidence of shrinkage is obtained from the bulk density. Bulk density values of 0.60 and 1.15 g/cm^3 were obtained for the KOH-aged and EtOH-aged samples, respectively. This compares to typical values of 0.9 g/cm^3 for this gel aged in EtOH and H_2O.

Average solvent layer thicknesses were calculated from the NMR-measured surface areas and the weights of solvent contained in the samples. The NMR surface area becomes suspect when the average layer thickness is less than ~0.3 nm because for fluid layers thinner than this, the two-phase fast-exchange model is no longer valid. Average solvent layer thicknesses ranged from 6.4 to 0.2 nm and from 3.1 to 0.1 nm for the EtOH- and KOH-aged samples, respectively. The difference in the maximum thickness is a result of different initial pore size distributions, and differences in the minimum thickness simply reflect the point when the experiment was stopped. On the basis of these calculations, the last three NMR surface areas for the EtOH-aged and the last two for the KOH-aged sample are suspect on an absolute basis.

After complete drying and before resaturation with ethanol, pore size distributions were obtained for each sample from analysis of nitrogen desorption isotherms. These pore size distributions are presented in Figure 4. For the EtOH-aged sample, significant pore volume apparently exists with pore size less than the 1-nm lower cutoff of Kelvin analysis. Also presented in Figure 4 are corresponding distributions obtained by completely resaturating the samples, performing a T_1 experiment, and using the α and β values obtained previously. Agreement between the two techniques is quite good considering that the NMR technique measures the distribution of hydraulic radii and N_2 condensation (desorption) is a measure of the pore constriction size and that NMR is sensitive to surface roughness and condensation is not. When the adsorption branch of the isotherm was used for condensation analysis, a broader pore size distribution is noted that is shifted to larger pore sizes (as expected). The fact that the NMR distributions are of slightly smaller pore size has two possible implications: the xerogel pore network is not highly constricted and/or the pores exhibit some degree of surface roughness. The effect of surface roughness can be envisioned by considering the hydraulic radius ($2V_p/A_s$) of a single cylindrical pore. If the pore is smooth, the hydraulic radius and the geometric radius are equivalent. However, if the pore surface is rough, the surface area will increase and result in a smaller hydraulic radius. As a result of the presence of the adsorbed film before condensation, N_2 condensation measurements will not be effected by changes in surface roughness (note: this is one reason why surface areas calculated from BET and integrating the pore size distribution rarely agree). The NMR pore size distribution for the EtOH-aged sample indicates the existence of microporous pore volume (approximately 36% of the pore volume) which is not observed in the KOH-aged sample. This microporosity would account for the EtOH-aged sample dry surface area being so much larger than that of the KOH-aged sample.

In addition to surface areas, the NMR data can also be used to obtain pore size distributions during drying. However, at some point in the drying the matrix stiffens such that it is no longer able to shrink with the decreasing amount of fluid, and the pores begin to become only partially saturated. Then it is no longer possible to derive pore size distributions. An estimation of this point can be made from the sample length and weight measurements during drying. Since only one length dimension was recorded during the drying, we assume that shrinkage is isotropic. Taking the initial pore volume as the initial fluid volume (determined gravimetrically), the total pore volume at any given point during the shrinkage can be calculated. The equation for determining the total pore volume at any sample length is

$$V/V_0 = \left[\frac{L - L_f}{L_0 - L_f}\right]^3 \tag{7}$$

where V = pore volume, V_0 = initial pore volume, L = sample length, L_f = sample length if completely dense (assuming 2.2 g/cm^3), and L_0 = initial sample length. The liquid volume in the sample can be determined for any point in the drying by calculating the difference between the recorded sample weight and the final dry sample weight. The point at which the pores are no longer completely saturated can thus be estimated by comparing the total pore volume (calculated from eq 7) with the measured fluid volume at various points during the drying. This comparison is shown in Figure 5 for the EtOH-aged and KOH-aged samples. The solid line represents the normalized pore volume as calculated from the length measurements and the initial fluid content via eq 7. The scattered points are fluid volumes calculated gravimetrically at different times during the drying. For the KOH-aged gel, the onset of pore draining is clearly seen to occur at a normalized length of 0.5, which corresponds to a ~75% solvent weight loss. For the EtOH-aged samples, it is difficult to pinpoint the deviation point. The error associated with the weights is fairly small, though the length measurements are more uncertain due to the measurement being taken through the glass NMR tube, resulting in some optical distortion. The conclusion of this analysis is that the gel pores can be confidently assumed completely full during the first 75% of weight loss. Cor-

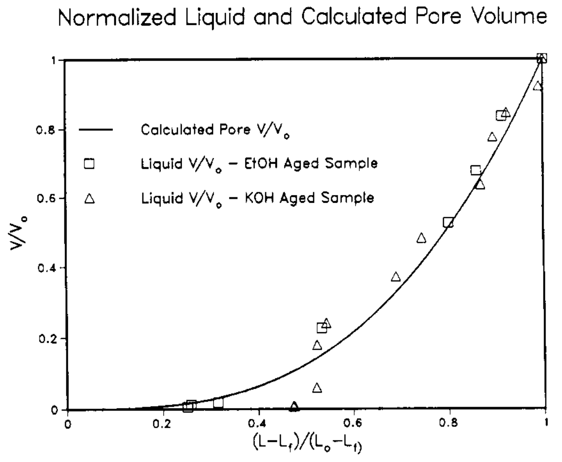

Figure 5. Variation of pore volume with sample length during drying.

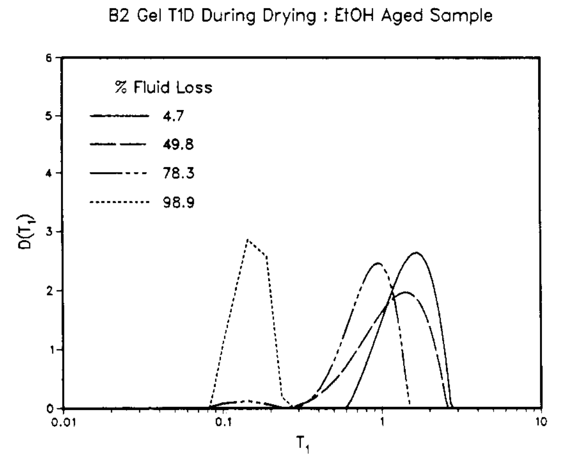

Figure 6. Distribution of relaxation times at different solvent contents for the EtOH-aged sample.

roborating evidence is seen in the surface area plot, Figure 3, where surface areas are observed to be constant until a marked decrease at approximaaely 78% fluid loss, possibly corresponding to the increased surface tension forces (which would tend to collapse small pores) present as the liquid meniscus begins to enter the gel matrix. At any point in the drying where the pores are still full, a pore size distribution can be extracted from NMR measurements if desired. After this point in the drying, just surface area, which depends only on a fluid layer thicker than approximately 0.3 nm, can be calculated. The final length for the KOH-aged sample is seen to be almost twice the length of the EtOH-aged sample, which is consistent with Figure 5 and indicates that the KOH-aged matrix is stiffer and thus less easily compressed by the capillary pressure during drying.

For each of the $T_{1_{\mathrm{av}}}$ values reported in Figure 1, a M(τ) relaxation data set is obtained that may be inverted by using the method of regularization to obtain the distribution of spin–lattice relaxation times. Figure 6 represents a family of distribution curves for the EtOH-aged sample calculated over a wide range of solvent content. Two points should be noted. As the solvent evaporates, the maximum in the distribution moves to smaller T_1. When the sample pores are no longer saturated, a second peak centered at $T_1 \approx 0.15$ s is observed. The first observation of this second peak corresponds to the region where deviations between the measured and observed shrinkage begin (Figure 5). For very dry samples, only a single peak centered at this T_1 is observed. We propose that this smaller peak is a direct measure of $T_{1_{\mathrm{surface}}}$. Since β is related to $T_{1_{\mathrm{surface}}}$ and the thickness of the surface-affected phase, Δ, knowing β and T_1, we can calculate a Δ value of 0.21 nm. This is in excellent agreement with previous reports of the surface-affected phase being 1–2 monolayers.[16,17] For each of the three lower percent solvent loss curves (Figure 6), a unique value of δ, the regularization smoothing parameter, was obtained: 0.015/4.7%, 0.002/49.8%, 0.0009/78.3%. For the driest sample (98.9% solvent loss), an optimum δ value was not obtained due to the poor signal-to-noise ratio. Therefore a value of 0.0009 was assumed. Since the actual δ value should be smaller, the distribution we present overpredicts the width of the distribution. Also, as part of the numerical solution of eq 2, the distributions presented in Figure 6 have been normalized and therefore do not reflect changes in pore volume.

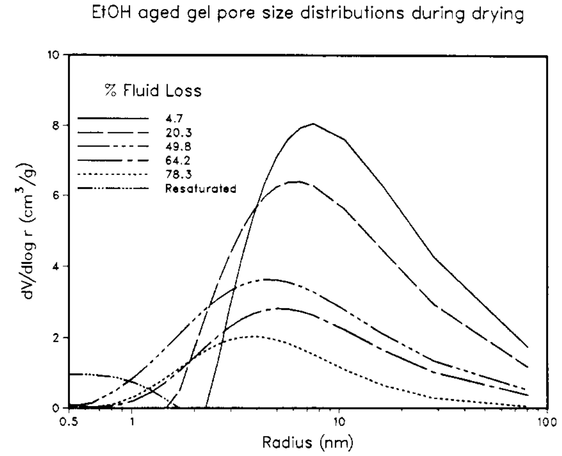

Figure 7. Pore size distributions at different solvent contents for the EtOH-aged sample.

T_1 distributions such as presented in Figure 6 may be combined with α, β, and the pore volume to obtain pore size distributions (PSD) during the drying process. Typical pore size distributions for the EtOH-aged sample are presented in Figure 7. Distribution corresponding to a range of drying are presented as well as the final dried sample, which has been resaturated. Optimum δ values were obtained for each curve: 0.015/4.7%, 0.0015/20.3%, 0.002/49.8%, 0.004/64.2%, 0.0009/78.3%, 0.0045/resaturated. During drying, the pore size continually moved to smaller pore sizes. The maximum in the PSD changed only from 6 to 3 nm during the first 80% of drying. However, the mean size decreases from ≈20 to ≈6 nm for this same degree of drying. During the last part of drying (80–100%), the sample's PSD undergoes dramatic collapse as the solvent meniscus penetrates the sample. In contrast, the KOH-aged sample exhibits significantly different behavior (see Figure 8). During the first 75% of drying the PSD shifts to smaller pore sizes and developing microporosity. However, in the last drying steps, the microporosity disappears and the PSD shows a slight increase.

Since the pore size distribution and surface area information presented above do not quite match what one would expect for isotropic shrinkage of smooth pores, we propose an alternative picture of the pore structure evolution process that accounts for these (previously unavailable) transient measures of pore structure. For isotropic pore shrinkage, one would expect the surface area to monotonically decrease during drying and that the pore size would scale with the decrease in pore volume to the one-third power. In general, our results indicate that until the drying front has penetrated the gel matrix, no major

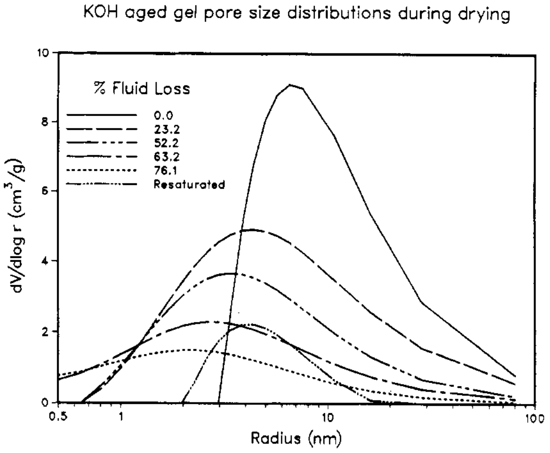

Figure 8. Pore size distributions at different solvent contents for the KOH-aged sample.

surface area change occurs and the pore radius, as determined via NMR, scales directly with pore volume. With respect to pore size, we note again that NMR results in the measurement of hydraulic radius (i.e., $r_p = 2V_p/A_s$). If the surface area is constant, the pore size should scale directly with pore volume, as is observed. The reason that the surface area undergoes no major change during the first 80% of drying is less clearcut. Apparently, the clusters forming the gel[23] undergo continued compaction during this first drying step without losing surface area. For example, this would result if additional branching during this step is minor, if there is relatively low coordination in the clusters and/or if the polymerization/depolymerization rate is low. In the final stages of drying, different mechanisms appear important for the KOH-aged and EtOH-aged samples. For the KOH-aged samples, the results may be interpreted as a stiff matrix that does not shrink under the influence of the capillary forces arising from the menisci penetrating the matrix. The pore volume becomes constant, but these large capillary forces result in the disappearance of surface roughness in the pores, resulting in a reduced surface area (and therefore, larger pore hydraulic radius). For the EtOH-aged sample, the matrix continues to shrink, resulting in very small final pore sizes (as observed with both NMR and N_2 desorption) and high surface area.

Acknowledgment. Support for this project has been provided by Sandia National Laboratories (Contract No. 02-2456 and 55-6778) under U.S. DOE Contract DE-04-76DP-00789. We thank S. Ross for the nitrogen adsorption measurements.

Nomenclature

A_s	specific surface area
$D(T_1)$	derivative of pore volume with respect to log (T_1)
$f(T_1)$	derivative of pore volume with respect to T_1
f_b	fraction of pore fluid with bulk fluid relaxation behavior
f_s	fraction of pore fluid with surface-affected relaxation behavior
L	sample length
L_0	initial sample length
L_f	sample length if completely dense
$\mathbf{M}(\tau)$	magnetization at time τ_1
$\mathbf{M}_0$	equilibrium magnetization
M_v	mass of solid sample/volume of fluid
r_p	hydraulic radius
T_1	spin–lattice relaxation time
$T_{1_{av}}$	average T_1
T_{1_b}	bulk fluid T_1
$T_{1_{min}}$	minimum expected T_1
$T_{1_{max}}$	maximum expected T_1
$T_{1_{surface}}$	T_1 of surface-affected phase
T_{1_s}	$T_{1_{surface}}/\Delta$
V	pore volume
V_0	pore volume before drying
V_p	specific pore volume
α	$1/T_{1_b}$
β	$2/T_{1_s}$
δ	optimum regularization smoothing parameter
Δ	thickness of surface-affected phase
τ	delay time between 180° and 90° pulses

Synthetic Study of Three Cesium Zirconates. Crystal Structure of Cs_2ZrO_3

Teng-Ming Chen and John D. Corbett*

Ames Laboratory—DOE[1] and Department of Chemistry, Iowa State University, Ames, Iowa 50011

Received June 9, 1988

The syntheses of cesium zirconates, potentially important sinks for fission-product cesium in Zircaloy-clad reactor systems, have been investigated for a diversity of reactions. The most effective synthetic routes involve reactions of elemental Cs and Zr with O_2 in open systems at slowly increasing temperatures or of finely divided ZrO_2 with Cs_2O (from Cs + CsO_2) in sealed silver tubing as the temperature is increased to 650–700 °C. Phase-pure Cs_2ZrO_3 has been obtained and shown to be isostructural with Cs_2PbO_3 (*Cmcm*, $Z = 4$, $a = 11.271$ (7) Å, $b = 7.743$ (4) Å, $c = 5.956$ (5) Å; R, R_w = 5.1, 5.8%). Two other cesium zirconates that contain a higher proportion of ZrO_2 have also been identified in mixtures produced by the second type of reaction. Their compositions have been estimated as $3Cs_2O{\cdot}7ZrO_2$ and $2Cs_2O{\cdot}7ZrO_2$ on the basis of the unit-cell volumes determined from single crystals of each together with known data for Cs_2ZrO_3 and the previously reported Cs_4ZrO_4.

Introduction

The identity and thermodynamic stability of any $m\mathrm{Cs_2O}{\cdot}n\mathrm{ZrO_2}$ phase are of prime importance with regard to the distribution of cesium, a major fission product, in Zircaloy-clad reactor fuel elements where there is an ample coating of ZrO_2 available on the cladding. The existence

0897-4756/89/2801-0040$01.50/0